

See discussions, stats, and author profiles for this publication at: <https://www.researchgate.net/publication/26765967>

Monitoring the Iron Status of the Ferroxidase Center of Escherichia coli Bacterioferritin Using Fluorescence Spectroscopy

ARTICLE in **BIOCHEMISTRY** · SEPTEMBER 2009

Impact Factor: 3.02 · DOI: 10.1021/bi900869x · Source: PubMed

CITATIONS

15

READS

28

6 AUTHORS, INCLUDING:



Allister Crow

University of Cambridge

19 PUBLICATIONS 401 CITATIONS

[SEE PROFILE](#)



Samina Yasmin

Habib University

4 PUBLICATIONS 137 CITATIONS

[SEE PROFILE](#)



Nick E Le Brun

University of East Anglia

86 PUBLICATIONS 2,085 CITATIONS

[SEE PROFILE](#)

Monitoring the Iron Status of the Ferroxidase Center of *Escherichia coli* Bacterioferritin Using Fluorescence Spectroscopy[†]

Tamara L. Lawson,[‡] Allister Crow,[§] Allison Lewin, Samina Yasmin, Geoffrey R. Moore, and Nick E. Le Brun*

Centre for Molecular and Structural Biochemistry, School of Chemistry, University of East Anglia, Norwich NR4 7TJ, U.K.

[‡]Current address: Department of Biochemistry and Molecular Biology, University of British Columbia, Life Sciences Centre, 2350 Health Sciences Mall, Vancouver, BC V6T 1Z3, Canada. [§]Current address: Department of Biological Chemistry, John Innes Centre, Norwich Research Park, Colney, Norwich NR4 7UH, U.K.

Received May 22, 2009; Revised Manuscript Received July 17, 2009

ABSTRACT: Ferritins solubilize and detoxify the essential metal iron through formation of a ferric mineral within the protein's central cavity. Key to this activity is an intrasubunit catalytic dinuclear iron center called the ferroxidase center. Here we show that the fluorescence intensity of *Escherichia coli* bacterioferritin (BFR), due to the presence of two tryptophan residues (Trp35 and Trp133) in each of the 24 subunits, is highly sensitive to the iron status of the ferroxidase center and is quenched to different extents by Fe²⁺ and Fe³⁺. Recovery of the quench following oxidation of Fe²⁺ to Fe³⁺ at the ferroxidase center was not observed, indicating that the di-Fe³⁺ form of the center is stable. Studies of the single-tryptophan variants W35F and W133F showed that Trp133, which lies ~10 Å from the ferroxidase center, is primarily responsible for the observed fluorescence sensitivity to iron, while studies of a stable *E. coli* BFR subunit dimer demonstrated that the observed quench properties are principally derived from the interaction of iron with tryptophan residues within the subunit dimer. A double-tryptophan variant (W35F/W133F) was found to exhibit fluorescence from the seven tyrosine residues present in each subunit, which was also sensitive to the iron status of the ferroxidase center. Finally, we demonstrate using Zn²⁺, a potent competitive inhibitor of Fe²⁺ binding and oxidation, that the fluorescence response can be used to monitor the loss of iron from the ferroxidase center.

Bacterioferritin (BFR) from *Escherichia coli* is a member of the widespread ferritin family of proteins that function in iron storage and detoxification (1–3). It consists of 24 identical subunits ($M_w \sim 18.5$ kDa for each) that are packed together to form an approximately spherical molecule with a central cavity, in which large amounts of iron can be deposited as a ferric-oxy-hydroxide-phosphate mineral core. In addition to the iron core, BFR contains up to 12 b-type heme groups, which are situated between symmetry-related subunit pairs, bound by two methionine residues (Met52 and Met52') (4), and a catalytic dinuclear iron site within each subunit, known as the ferroxidase center. The two iron ions are bridged by two carboxylates, and each has monodentate carboxylate and histidine ligands (5) (see Figure 1).

The ferroxidase center plays a key role in mineralization (6, 7), which proceeds through the binding of Fe²⁺ ions at the vacant ferroxidase centers (phase 1), the rapid reaction with oxygen (or hydrogen peroxide) to generate a bridged di-Fe³⁺ center and reduced oxygen species (phase 2) (6–8), and slow core formation (phase 3). In related mammalian ferritins, the ferroxidase center also plays a key role in mineralization, but it is not absolutely required for this process; in the absence of a functional center, core nucleation can still occur, albeit very slowly, but once a

sufficiently large core surface has formed, surface-catalyzed oxidation can occur and core formation rates recover to near wild-type levels (9). BFR has quite different mechanistic features compared to eukaryotic ferritins; its ferroxidase center is active and absolutely required throughout core formation (10), indicating that the core surface alone cannot sustain significant rates of Fe²⁺ oxidation.

Recently, high-resolution structures of apo, di-Fe²⁺, and bridged di-Fe³⁺ forms of the *E. coli* BFR ferroxidase center have been determined, and a functionally important Fe²⁺-binding site has been identified on the inner surface of the BFR cavity, ligated only by His46 and Asp50 (5). The available data support a model of mineralization in which the ferroxidase center continually cycles between ferrous and ferric forms, leading to oxygen reduction, with the electrons required to reduce the Fe³⁺ at the center coming from Fe²⁺ bound to the core surface (5, 10).

Tryptophan fluorescence emission of H- and L-chain mammalian ferritins has previously been shown to be sensitive to the iron status of the protein and, in particular, to that of the ferroxidase centers (of homopolymer H-chain ferritin and of horse spleen ferritin, which typically contains 10–15% H-chain subunits) (11). Mammalian ferritin subunits contain a single tryptophan residue, which, in H-chain ferritins, is located ~12 Å from the ferroxidase center. *E. coli* BFR contains two tryptophan residues per subunit, Trp35 and Trp133, the latter of which is located within ~10 Å of the ferroxidase center (see Figure 1). Therefore, it was of great interest to determine whether the fluorescence properties of BFR could be exploited as a

[†]This work was supported by the UK's BBSRC through the award of Grant BB/D001943/1 to N.E.L.B. and G.R.M. and of a studentship to T.L.L.

*To whom correspondence should be addressed. E-mail: n.le-brun@uea.ac.uk. Phone: +44 1603 592699. Fax: +44 1603 592003.

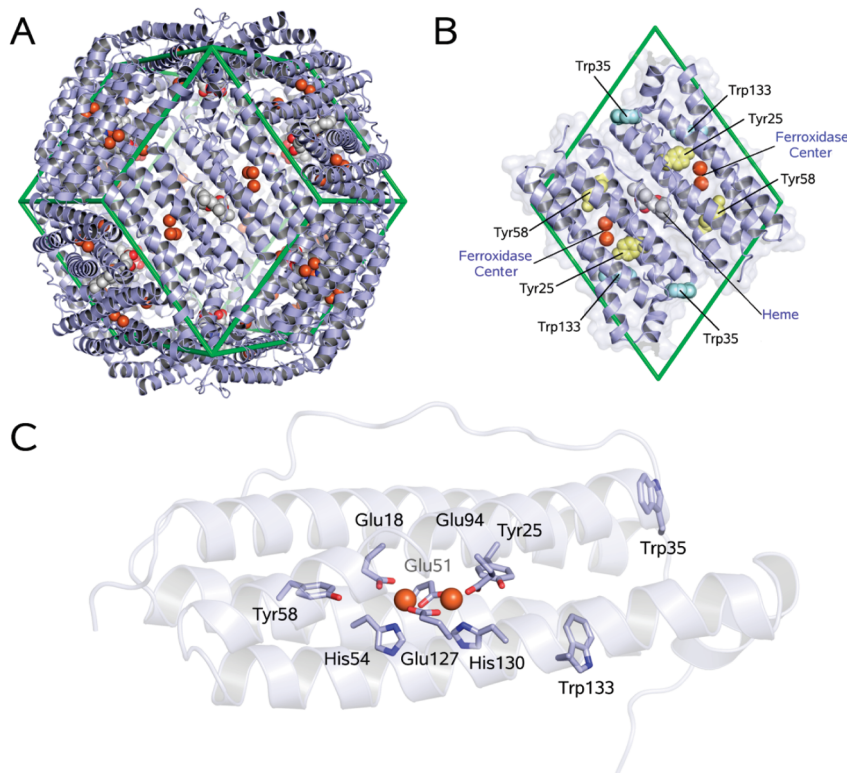


FIGURE 1: Molecular architecture of BFR. (A) BFR 24-mer superposed on a three-dimensional rhombic dodecahedron (green) to emphasize the symmetric assembly of subunits. (B) Subunit dimer of BFR corresponding to a single rhombic face of the 12-sided dodecahedron. (C) Detail of the ferroxidase center in a single subunit. All structural figures in this panel were generated using coordinates from Protein Data Bank entry 3E1M.

mechanistic probe of Fe^{2+} binding and oxidation, particularly as fluorescence offers the potential to measure processes that cannot be followed by absorbance spectroscopy. Here, we report studies of the fluorescence properties of wild-type BFR and those of single- and double-tryptophan variants, and their responses to Fe^{2+} binding and oxidation. We demonstrate that fluorescence spectroscopy provides a sensitive method of monitoring Fe^{2+} binding and oxidation events in BFR, as the tryptophan fluorescence of the protein is highly sensitive to the presence and oxidation state of iron at the ferroxidase center and therefore offers a precise spectroscopic probe of the mechanism of iron incorporation. Oxidation of Fe^{2+} at the ferroxidase center was found to be the major cause of fluorescence quenching. Fluorescence intensity did not recover following Fe^{2+} oxidation, indicating clearly that Fe^{3+} remained at the ferroxidase center. Recovery of fluorescence intensity was observed, however, upon addition of Zn^{2+} , a well-known inhibitor of ferroxidase activity that binds tightly and specifically at the ferroxidase center. The data support a recently proposed mechanism for iron core mineralization in BFR in which the ferroxidase center cycles between di- Fe^{2+} and bridged di- Fe^{3+} forms, thereby acting as a true catalytic center, rather than as a pore for the conduit of Fe^{3+} ions into the BFR central cavity. Furthermore, fluorescence spectroscopy is revealed to be a highly sensitive and selective probe of the iron status of the ferroxidase center and therefore offers new insight into the role of the ferroxidase center in the mechanism of mineralization in BFR.

EXPERIMENTAL PROCEDURES

Strains, Growth Media, and Site-Directed Mutagenesis. *E. coli* strains JM109 and BL21(DE3)pLysS (Promega) were used for site-directed mutagenesis and expression, respectively,

and grown at 37 °C in LB¹ (Luria-Bertani) broth, on LA plates consisting of LB broth with 1.25% (w/v) agar or in M9 minimal medium. Ampicillin, where appropriate, was used at a concentration of 100 mg/L. Molecular genetics techniques were used as previously described (12). Plasmid DNA was isolated using commercial mini- or midprep kits (Qiagen). Enzymes for DNA manipulation were purchased from Roche or Promega. Site-directed mutagenesis was conducted using a whole-plasmid method (13). For the generation of constructs producing W35F and W133F BFR, primers CGAATTAAAAACTTGGTCT-CAAACGTC and GGCCATATCGACTTCTGGAAACGGAAC and their respective reverse complements were used with pGS578 as a template, giving pTLN1 and pTLN2, respectively. For W35F/W133F BFR, the W35F primer was used with pTLN2, generating pTLN5. The *NdeI*-*EcoRI* fragment of each was cloned into pET21a giving pTLN3 (W35F), pTLN4 (W133F), and pTLN6 (W35F/W133F), each of which was confirmed by sequencing (MWG Biotech).

Protein Purification and Removal of Non-Heme Iron. Wild-type and tryptophan variants of BFR were purified, and non-heme iron was removed as previously described (10, 14). Heme contents of non-heme iron-free proteins, determined through the heme Soret absorbance intensity, using an ϵ_{418} of 107000 M⁻¹ cm⁻¹, were found to be ~1 per 24mer for the wild type and ~1.5 per 24mer for W35F, W133F, and W35F/W133F BFRs, respectively. Concentrations of wild-type and tryptophan variants of BFR were calculated using the following per subunit ϵ_{280} values: 33000 M⁻¹ cm⁻¹ [wild type (8)], 22300 M⁻¹ cm⁻¹

¹Abbreviations: LB, Luria-Bertani; Mes, 2-(*N*-morpholino)-ethanesulfonic acid; Mops, 3-(*N*-morpholino)propanesulfonic acid; FRET, fluorescence resonance energy transfer; PDB, Protein Data Bank.

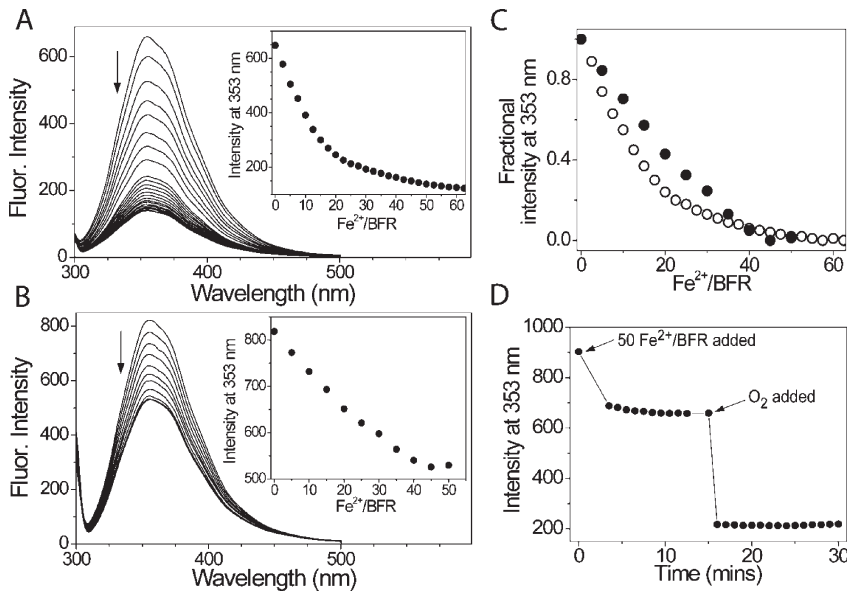


FIGURE 2: Wild-type BFR Fe^{2+} binding and oxidation monitored by fluorescence spectroscopy. (A and B) Fluorescence emission titrations of wild-type BFR with Fe^{2+} ions under aerobic (A) and anaerobic (B) conditions. Excitation was at 290 nm (with excitation and emission slits of 12 and 6 nm, respectively). BFR [0.05 (A) and 0.1 μM (B)] was in 0.1 M Mes (pH 6.5), at 25 °C. The insets in panels A and B are plots of emission intensity at 353 nm as a function of the number of Fe^{2+} ions per BFR. (C) Plot of fractional intensity at 353 nm for aerobic (\circ) and anaerobic (\bullet) titrations. (D) Plot of emission intensity at 353 nm of wild-type BFR as a function of time before and after the anaerobic addition of 50 Fe^{2+} ions per BFR. At the arrowed time point, the sample was exposed to air and further I_{353} measurements were taken.

(W35F), 23375 $\text{M}^{-1} \text{cm}^{-1}$ [W133F(5)], 18665 $\text{M}^{-1} \text{cm}^{-1}$ (W35F/W133F), determined by amino acid analyses (Alta Bioscience). The *E. coli* BFR subunit dimer was prepared as previously described (15), and its concentration was determined using a per subunit ϵ_{280} value of 33000 $\text{M}^{-1} \text{cm}^{-1}$ (8).

Spectroscopic Methods. Fluorescence emission spectra were recorded using a Perkin-Elmer LS55 spectrophotometer at 25 °C with excitation at 290 nm (for tryptophan excitation) or 276 nm (for tyrosine excitation). Excitation and emission slit widths were varied depending on the emission intensity of the sample. Metal ion additions were made using a microsyringe (Hamilton). For anaerobic experiments, additions were made in an anaerobic glovebox (Faircrest Engineering) in which the oxygen concentration was <2 ppm. For aerobic experiments, air-saturated solutions were employed, in which the concentration of oxygen was far in excess of that of iron. For experiments in which oxygen was introduced into a previously anaerobic sample, this was achieved by repeated aspiration of the sample, using a pipettor, under aerobic conditions. Titration experiments were conducted using a sample cuvette only, and after each Fe^{2+} addition, samples were incubated for 5 min before spectra were recorded. Data were corrected for dilution effects and plotted as either absolute intensity (arbitrary units) or as fractional intensity $[(I_t - I_f)/(I_i - I_f)]$, where I_t is the intensity at point t in the titration and I_i and I_f are the initial and final intensity values, respectively].

Kinetic Methods. Kinetic measurements of changes in absorption at 340 nm after the addition of Fe^{2+} (as ferrous ammonium sulfate) to wild-type apo-BFR and apo-BFR variants were made using either a conventional UV-visible spectrophotometer (Perkin-Elmer λ35 or λ800 spectrophotometer), for which additions to the sample were made using a microsyringe (Hamilton), or by using a stopped-flow apparatus (Applied Photophysics DX17MV) with the BFR solution in one syringe and the metal ion solution in another.

Structural Methods. Prior to crystallization, W35F and W133F BFR proteins were pretreated aerobically with

$\text{Fe}(\text{II})(\text{NH}_4)_2(\text{SO}_4)_2$ to a level of 48 Fe^{2+} ions per 24mer protein, concentrated to ~10 mg/mL in 20 mM Mes (pH 6.5), and centrifuged at 13000 rpm for 5 min to remove particulate matter. Crystals were obtained using the sitting drop vapor diffusion method at 16 °C. Sitting drops (2 μL) were formed from equal volumes of the protein solution and crystallization reagent and equilibrated over an 800 μL volume of the reagent alone. The crystallization reagent consisted of 1.8 M ammonium sulfate and 0.1 M trisodium citrate (pH 5.0). Crystals were cryoprotected and frozen in a solution of 1.65 M ammonium sulfate, 0.1 M Mops (pH 7.0), and 25% glycerol. X-ray diffraction data were collected at the UK Synchrotron Radiation Source (SRS), station 10.1. The structures of W35F and W133F BFR were determined by molecular replacement using the recently reported apo-BFR structure [PDB entry 3E1J (5)] as a starting point for refinement. Structural figures were produced using PYMOL (16) and annotated with GIMP. Coordinates and associated structure factor amplitudes (including anomalous data) were deposited in the RCSB PDB as entries 3GHQ (W35F) and 3E1Q (W133F).

RESULTS AND DISCUSSION

Fe^{2+} Binding and Fe^{2+} Oxidation Quench the Tryptophan Fluorescence of BFR to Different Extents. Wild-type BFR lacking non-heme iron (apo-BFR) exhibited an intense fluorescence emission band at 353 nm due to the two tryptophan residues in each of its 24 subunits. To investigate the effect of iron on the fluorescence properties of the protein, apo-BFR was titrated with Fe^{2+} ions under aerobic conditions (see Figure 2A), which resulted in a quenching of the fluorescence emission intensity. Recent structural studies of *E. coli* BFR in iron-free (apo) and Fe^{2+} - and Fe^{3+} -bound forms revealed very few structural changes upon Fe^{2+} binding or oxidation, leading to the conclusion that the ferroxidase center, in its apo form, is preformed, ready to accept incoming Fe^{2+} ions (5). Therefore, the effect on the fluorescence intensity results simply from the binding of an efficient fluorescence quenching agent close to the

protein fluorophore(s). In contrast to a similar titration measured by UV-visible absorbance at 340 nm (7), in which Fe^{2+} oxidation is monitored directly through charge transfer bands due to O_2^-/OH^- -coordinated Fe^{3+} , a plot of intensity as a function of Fe^{2+} was not linear (up to 48 Fe^{2+} ions per protein). Instead, the plot (inset, Figure 2A) was curved, although saturation was still observed at ~ 50 Fe^{2+} ions per BFR (~ 2 Fe^{2+} ions per BFR subunit), at which point the emission intensity was reduced to $\sim 20\%$ of its original value. A curved rather than linear response was observed most likely because Fe^{2+} binding or oxidation causes quenching of fluorescence intensity in neighboring subunits. Thus, Fe^{2+} binding or oxidation in the latter part of the titration would not cause the same degree of quenching as the initial binding or oxidation of Fe^{2+} (because intensity has already been significantly quenched by earlier additions).

Once it had been established that fluorescence intensity is sensitive to iron, it was important to determine the relative contributions of Fe^{2+} and Fe^{3+} . To do this, apo-BFR was titrated in a fashion similar to that described above but under anaerobic conditions so that experiments in which Fe^{2+} binding and oxidation (to Fe^{3+}) occurred could be compared with those in which Fe^{2+} binding but not oxidation occurred. First, the anaerobic fluorescence emission spectrum of apo-BFR established that molecular oxygen alone did not cause a quenching of intensity (not shown). Following the addition of Fe^{2+} , however, quenching was observed (see Figure 2B). The plot of intensity as a function of Fe^{2+} added (inset, Figure 2B) was very different from that under aerobic conditions (compare to Figure 2A), indicating that both Fe^{2+} binding and Fe^{2+} oxidation cause quenching. A similar conclusion was drawn from studies of mammalian H-chain ferritin (11). The anaerobic Fe^{2+} plot was also curved [but less so than the aerobic plot (see Figure 2C, in which fractional intensity changes are plotted)], with saturation observed at ~ 45 Fe^{2+} ions per BFR, at which point $\sim 65\text{--}70\%$ of the original intensity remained.² This indicated that although both the binding of Fe^{2+} and its subsequent oxidation are both significant contributors to the observed quench, the oxidation step is the major one.

To further investigate the distinct effects of Fe^{2+} binding and oxidation on the tryptophan fluorescence intensity, 50 Fe^{2+} ions were added to apo-BFR under anaerobic conditions and the intensity at 353 nm was followed as a function of time (see Figure 2D). Oxygen was subsequently introduced and the effect on the 353 nm intensity followed. These data clearly resolved the anaerobic and aerobic contributions for a single sample and confirmed that the presence of Fe^{3+} ions at the ferroxidase center is the major contributor to quenching of the fluorescence. Furthermore, we note that following the introduction of oxygen and associated oxidation of Fe^{2+} to Fe^{3+} there was no further change in fluorescence, indicating that Fe^{3+} remains at the ferroxidase center, such that the bridged di- Fe^{3+} form of the center is stable, consistent with previous mechanistic and structural studies (5, 8).

²Although the anaerobic plot appears to represent a binding isotherm, from which a dissociation constant might be obtainable, attempts to fit the data to a simple binding process indicated a K_d value in the nanomolar range, with a stoichiometry of ~ 35 Fe^{2+} ions per 24mer. Neither of these values is consistent with previous studies: 2 Fe^{2+} ions bind per ferroxidase center (5, 7), and Zn^{2+} binds to BFR with a K_d of $\sim 1 \times 10^{-7}$ M and is a potent inhibitor of ferroxidase activity because it binds at the center with a significantly higher affinity than Fe^{2+} (6, 17). The fit parameters are a consequence of the fact that Fe^{2+} binding to BFR does not result in a linear quench response, as described in the text.

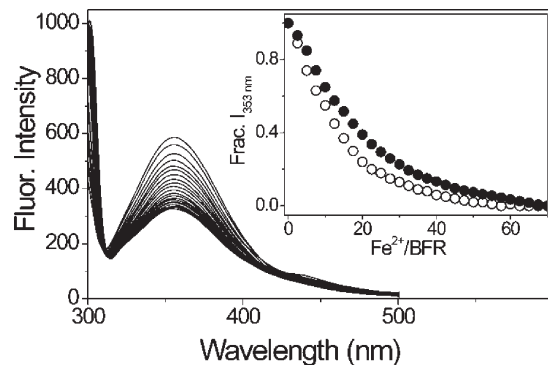


FIGURE 3: BFR subunit dimer Fe^{2+} binding and oxidation monitored by fluorescence spectroscopy. Fluorescence emission titration of the BFR subunit dimer with Fe^{2+} ions under aerobic conditions. Excitation was at 295 nm (with excitation and emission slits of 12 and 6 nm, respectively). The BFR subunit dimer ($1.2 \mu\text{M}$) was in 0.1 M Mes (pH 6.5), at 25°C . The inset is a comparison plot of fractional intensity at 353 nm for aerobic Fe^{2+} titrations of the BFR subunit dimer (●) and wild-type BFR (○) as a function of Fe^{2+} per 24mer (i.e., the dimer is represented as the 24mer in terms of concentration).

The Majority of the Fe^{2+} - and Fe^{3+} -Induced Fluorescence Quench Occurs within Each Subunit Dimer. BFR consists of 24 identical subunits arranged as 12 subunit dimers. To determine the extent to which iron bound within one subunit dimer influences the fluorescence properties of another subunit, we employed an engineered version of *E. coli* BFR that does not assemble beyond a dimer of subunits but retains the ability to bind Fe^{2+} and catalyze its oxidation (15, 18). An aerobic titration, similar to that described above for the 24mer protein, was conducted with the BFR subunit dimer. Changes in the fluorescence spectrum with an increasing level of Fe^{2+} are shown in Figure 3 along with a plot of fractional intensity at 353 nm as a function of Fe^{2+} added per BFR (expressed, in terms of concentration, as the 24mer protein to enable a direct comparison). This revealed that Fe^{2+} binding and oxidation caused a significant quench, with $\sim 35\%$ of the original intensity remaining at the end point. This was somewhat higher than in the wild-type 24mer protein (see Figure 2B), indicating that some of the observed quench in the 24mer must result from interactions that occur between subunit dimers. The shape of the plot was also somewhat different from the equivalent plot for the 24mer (inset, Figure 3). We also noted that, in the dimer sample, intensity continued to decrease beyond ~ 48 Fe^{2+} (i.e., ~ 4 per dimer), indicating that further Fe^{2+} ions can bind to the surface of the dimer, as previously reported (15), where they cause further minor quenching. Data from the 24mer did not indicate quenching beyond 2 irons per subunit, even though further binding of Fe^{2+} at an inner surface site has been observed crystallographically (5). This may be a consequence of the fact that the extent of the quench was less significant in the subunit dimer (and so “quenchable” intensity remained at 2 irons per subunit, whereas it may not in the 24mer because of additional quenching due to intersubunit dimer interactions). Despite these differences, it appears that the most significant contributions to the quench are derived from interactions within the subunit dimer.

The subunit dimer data provide significant information about Fe^{2+} binding and oxidation and, in particular, about whether this occurs cooperatively within the subunit dimer. If positive cooperativity existed between the ferroxidase centers of the two subunits of the dimer, we would have expected to observe a linear quench response, as Fe^{2+} binding and oxidation at one center

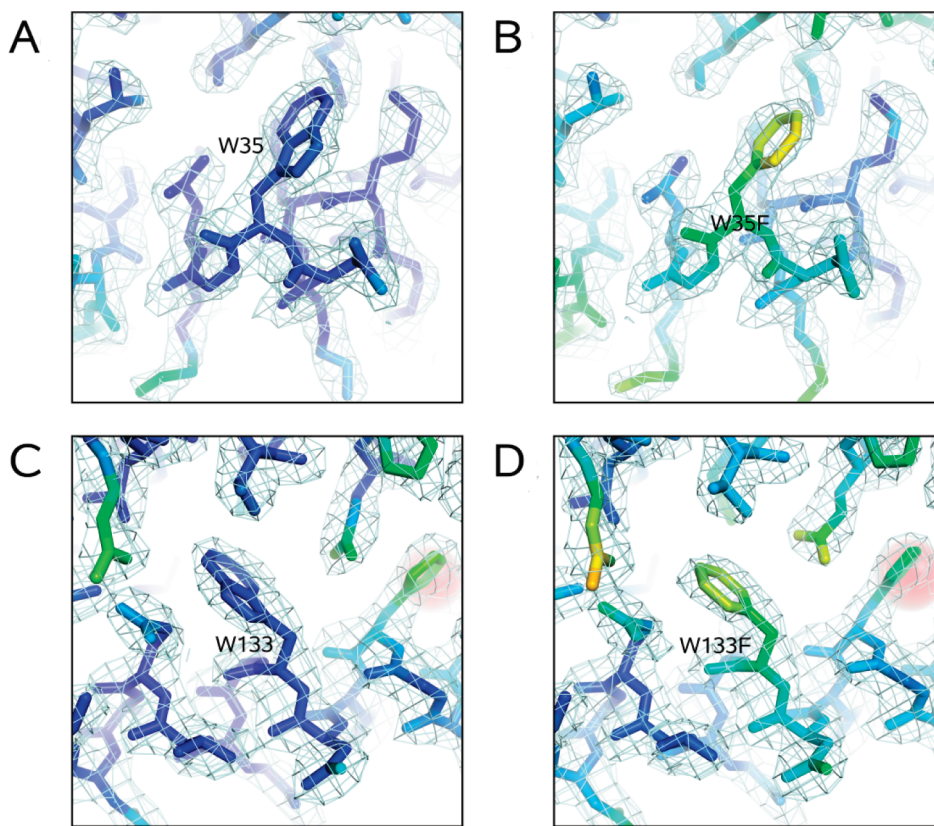


FIGURE 4: Structures of tryptophan-to-phenylalanine variants in comparison with the wild-type structure: (A) Trp35 in wild-type BFR, (B) W35F variant BFR, (C) Trp133 in wild-type BFR, and (D) W133F variant BFR. All atoms are colored by *B* factor, with blue indicating a low degree of thermal motion and yellow/red indicating a higher degree of motion.

would favor binding and oxidation at the other center of the dimer over binding at an unoccupied subunit dimer.³ Because a curved response was observed, we can rule out the possibility that strong positive cooperativity in Fe^{2+} binding and oxidation exists between subunits of the dimer. The data do not enable us to distinguish between cooperative and noncooperative binding and oxidation of Fe^{2+} within a single ferroxidase center, although previous data indicated that at least oxidation occurs cooperatively as oxygen or hydrogen peroxide reacts with the di- Fe^{2+} form of the center (6–8).

³Addition of a substoichiometric amount of Fe^{2+} to the apo-BFR subunit dimer would result in the initial binding of Fe^{2+} at one of the two ferroxidase centers, causing a significant quench of the fluorescence due to both monomers of the dimer. Further added Fe^{2+} can then either bind randomly at unoccupied centers or cooperatively (positive or negative), where the binding affinity of one ferroxidase center of the subunit dimer is affected by the iron status of the other center. In the case of strong positive cooperativity, both ferroxidase centers of a single subunit dimer molecule would be filled before any of the remaining apo subunit dimers bound Fe^{2+} . Because binding or oxidation of Fe^{2+} at one ferroxidase center affects the fluorescence of the subunit to which it belongs and the other subunit of the dimer, the different binding models would result in quite different titration behavior. Both noncooperative (random) and negatively cooperative binding would result in a rapid decrease in intensity, as more and more of the subunit dimers would contain at least some (quenching) iron. This is what was observed experimentally. Note that the noncooperative and negatively cooperative situations cannot be easily distinguished. On the other hand, positively cooperative binding would result in there always being at least some apo-BFR present, right up to the point of saturation of the ferroxidase centers. In this case, the presence of the strongly fluorescent apo-BFR subunit dimer would cause the fluorescence intensity to decrease more steadily as more Fe^{2+} is added. In the limit of strong positive cooperativity, the observed decrease would be essentially linear as only fully occupied and fully apo forms of the subunit dimer would be present.

The Fluorescence Due to Trp133 in Wild-Type BFR Is Significantly Quenched. Each BFR subunit contains two tryptophan residues. One of these, Trp133, is located within 10 Å of the ferroxidase center, while the other, Trp35, is more remote. To resolve the relative contributions of Trp35 and Trp133 to BFR fluorescence, W35F, W133F, and W35F/W133F BFR proteins were generated and purified. W35F and W133F BFRs were crystallized, and their structures were determined by molecular replacement methods. Data collection and refinement statistics are given in Table S1 of the Supporting Information. Structures of W35F and W133F are shown in juxtaposition to the wild-type structure in Figure 4. In both W35F and W133F, the substitution of tryptophan with phenylalanine resulted in very little structural change beyond the affected residue itself. In both cases, the aromatic ring of the phenylalanine occupies the same space as the indole ring of the tryptophan wild type; however, because of the slightly smaller size of the phenyl ring, the phenylalanine variants have slightly more freedom to vibrate, giving slightly higher *B* factors than in the wild type (Figure 4). The structures thus confirmed that mutation did not significantly disrupt the structure of the BFR variants. Fluorescence spectra were recorded for both single variants and for the double W35F/W133F BFR variant (Figure 5A). The intensity of W35F (i.e., due to the remaining tryptophan, Trp133) was significantly lower than that of W133F (due to Trp35). The combined intensities of the two single-tryptophan variants were approximately equal to that of the wild-type protein, indicating that Trp133 exhibits quenched fluorescence in wild-type BFR. This is supported by fluorescence data for the wild-type and variant proteins under denaturing conditions (see Figure 5B). The intensity due to wild-type BFR and

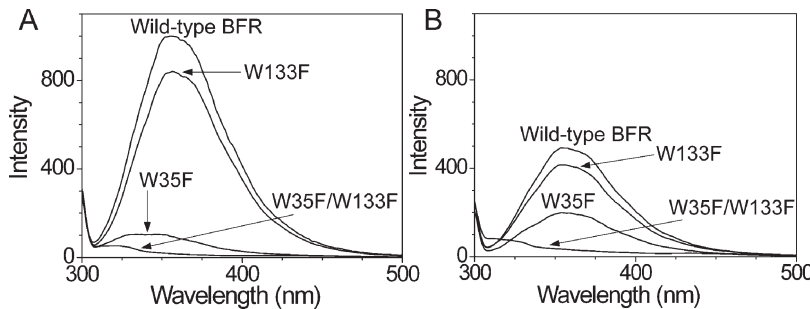


FIGURE 5: Fluorescence properties of wild-type and BFR tryptophan variants. (A) Fluorescence emission spectra of wild-type, W35F, W133F and W35F/W133F BFR, as indicated. BFR and variant proteins ($0.1 \mu\text{M}$) were in 0.1 M Mes (pH 6.5), at 25 °C. Excitation was at 290 nm (with excitation and emission slits of 10 and 5.5 nm, respectively). (B) Like panel A except that proteins were in 6 M Gdn-HCl and 0.1 M Mes (pH 6.5).

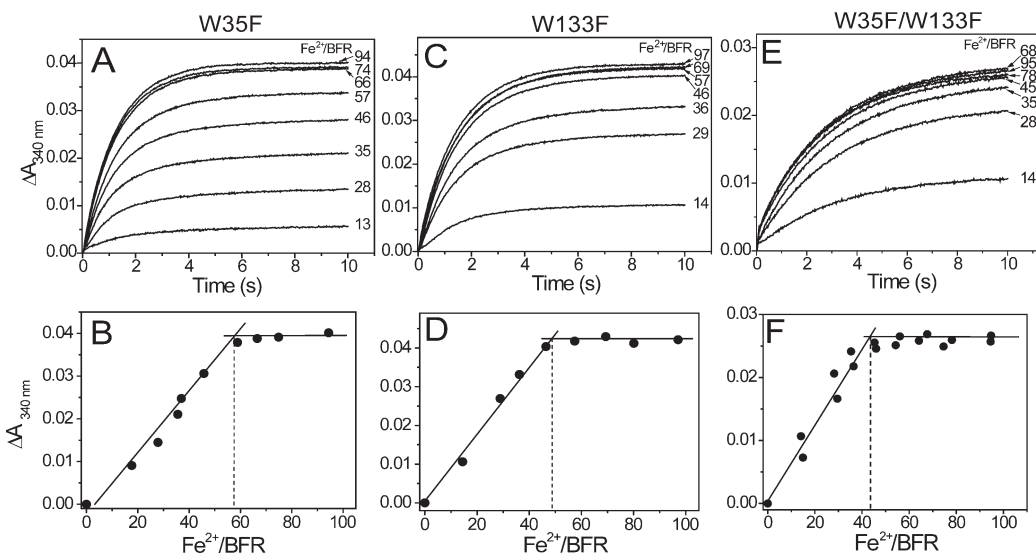


FIGURE 6: Functional properties of BFR tryptophan variants. Absorption changes at 340 nm in the first 10 s measured by stopped-flow following additions of Fe^{2+} to (A) W35F BFR, (C) W133F BFR, and (E) W35F/W133F BFR in the stoichiometric range of 0–100 Fe^{2+} ions per BFR, as indicated. BFR proteins (final concentration of $0.5 \mu\text{M}$) were in 0.1 M Mes (pH 6.5), at 25 °C. (B, D, and F) Plots of absorption changes at 340 nm, corresponding to phase 2 Fe^{2+} oxidation, as a function of the $\text{Fe}^{2+}/\text{BFR}$ ratio for W35F, W133F, and W35F/W133F BFR, respectively. Saturation of phase 2 is indicated by the intersection of initial and final linear regions of the plots. Data for panels B, D, and F were derived from panels A, C, and E, respectively, and from equivalent experiments.

W133F BFR (containing Trp35) was quenched upon unfolding, while that for W35F BFR (containing Trp133) increased upon unfolding. The double variant retained fluorescence intensity, but this was much weaker and was shifted to ~ 310 nm, characteristic of tyrosine fluorescence. Therefore, the data show that the majority of fluorescence intensity in wild-type apo-BFR is derived from Trp35.

The Fluorescence Response of Wild-Type BFR to Fe^{2+} and Fe^{3+} Is Mediated via Trp133. Once it had been established that the two tryptophan residues of BFR do not contribute equally to fluorescence intensity, it was important to determine their relative contributions to the fluorescence sensitivity of wild-type BFR to Fe^{2+} binding and oxidation. To do this, it was first necessary to determine whether their initial Fe^{2+} binding and oxidation activities were altered from those of wild-type BFR. Initial Fe^{2+} oxidation at the ferroxidase center of BFR has been well characterized previously using stopped-flow rapid kinetic methods (6, 7, 19), and this method was also used here. Kinetic traces very similar to those previously reported for wild-type BFR were observed for both W35F and W133F BFR (Figure 6A, C), demonstrating that the rate of initial Fe^{2+} oxidation at the ferroxidase center in these variants was essentially unaffected.

For the W35F/W133F double variant, data indicated that phase 2 oxidation occurred at a slightly reduced rate and resulted in an overall absorption change smaller than that observed for the wild type or either single-tryptophan variant (Figure 6E). However, plots of ΔA_{340} as a function of Fe^{2+} ions per BFR (Figure 6B, D, F) showed clearly that the phase 2 saturation characteristics of all three variants were unaffected; i.e., 2 Fe^{2+} ions are rapidly oxidized per BFR subunit, and we conclude that the initial binding and oxidation of Fe^{2+} at the ferroxidase center of each variant protein were not significantly altered relative to that of the wild-type protein. Thus, these variants were validated as potentially useful probes of the contribution of each of the tryptophan residues to the quenching behavior of the wild-type protein.

The single-tryptophan variants were titrated under aerobic conditions, as described above for the wild-type protein. Figure 7A shows changes in the fluorescence spectrum following aerobic additions of Fe^{2+} to W35F BFR. In this variant, the major contributor to the wild-type protein's fluorescence intensity (Trp35) was not present, so the absolute intensity due to the variant was significantly lower than that of the wild type (see Figure 2). However, the extent to which the initial intensity was

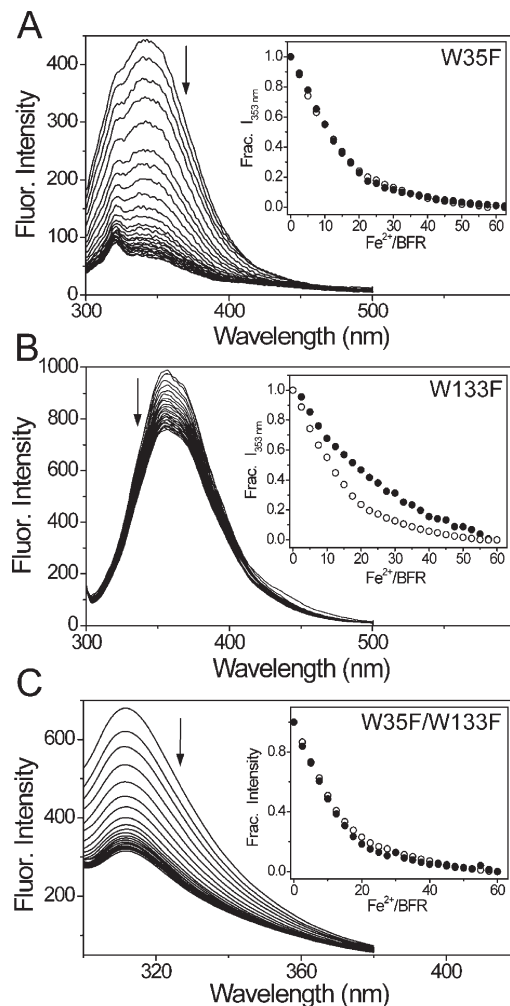


FIGURE 7: Fluorescence properties of BFR tryptophan variants. Sensitivities to Fe^{2+} and Fe^{3+} . Plots of fluorescence emission intensity at 353 nm as a function of Fe^{2+} per W35F BFR (A) and W133F BFR (B) under aerobic conditions. Excitation was at 290 nm (with excitation and emission slits of 12 and 16 nm, respectively, for W35F BFR and 10 and 6 nm, respectively, for W133F BFR). (C) Plot of fluorescence emission intensity at 310 nm as a function of Fe^{2+} per W35F/W133F BFR under aerobic conditions. Excitation was at 280 nm (with excitation and emission slits of 12 and 6 nm, respectively). Insets are comparison plots of fractional intensity at 353 nm as a function of Fe^{2+} per protein. Variant BFR data are shown as filled circles, and wild-type data (empty circles) are shown to aid comparison. Proteins ($0.1 \mu\text{M}$) were in 0.1 M Mes (pH 6.5), at 25°C .

quenched was essentially identical to that observed for the wild-type protein: $\sim 20\%$ of the intensity remained after the addition of 50 Fe^{2+} ions per protein (Figure 7A). A plot of relative emission intensity at 353 nm as a function of iron per protein (inset, Figure 7A) showed that the shape of the plot was remarkably similar to that of the wild-type protein (plotted to aid comparison). Figure 7B shows the equivalent data for W133F BFR. The initial absolute intensity due to the variant was similar to that of the wild-type protein (because Trp133 provides only a minor contribution to the overall fluorescence), but the extent of the quench was much smaller than in wild-type (or W35F) BFR, with $\sim 78\%$ of the initial intensity remaining after the addition of 50 Fe^{2+} ions per protein. The shape of the plot was also very different, and the quench was not saturated at 50 Fe^{2+} ions per protein (see the inset of Figure 7B). From these data, it is clear that Trp133 is much more sensitive to Fe^{2+} binding and oxidation than Trp35 is, consistent with the fact that Trp133 is closer to the ferroxidase center. Titration experiments conducted under anaerobic conditions, which assessed the sensitivity of the proteins to Fe^{2+} binding alone (see Figure S1 of the Supporting Information), were entirely consistent with this.

Therefore, we conclude that Trp133, which exhibits significantly quenched fluorescence intensity in the apo wild-type protein, is principally responsible for the sensitivity of the protein to iron. In its absence (i.e., in the W133F variant), the initial fluorescence intensity (due to Trp35) was similar to that of the wild-type protein, and this was not greatly affected by the addition of Fe^{2+} or its oxidation to Fe^{3+} . This is consistent with Trp35 being $\sim 20 \text{ \AA}$ from the ferroxidase center. In the absence of Trp35 (i.e., in the W35F variant), the remaining Trp133 residue remained partly quenched, via an unknown, iron-independent mechanism, but also remained highly sensitive to both Fe^{2+} and its oxidation to Fe^{3+} .

The data indicated that the observed response of the wild-type protein must arise from a fluorescence resonance energy transfer (FRET) mechanism between Trp133 and Trp35, which results in significant quenching of the fluorescence intensity originating from the remote Trp35 residue. In the absence of Trp133, FRET cannot occur and Fe^{2+} and Fe^{3+} have a much less significant effect on the fluorescence intensity. The two tryptophan residues are separated by $\sim 12 \text{ \AA}$, well within the range for efficient FRET (20).

Fe^{2+} Binding and Oxidation Can Be Followed via Tyrosine Fluorescence in a Tryptophan-Free BFR Variant.

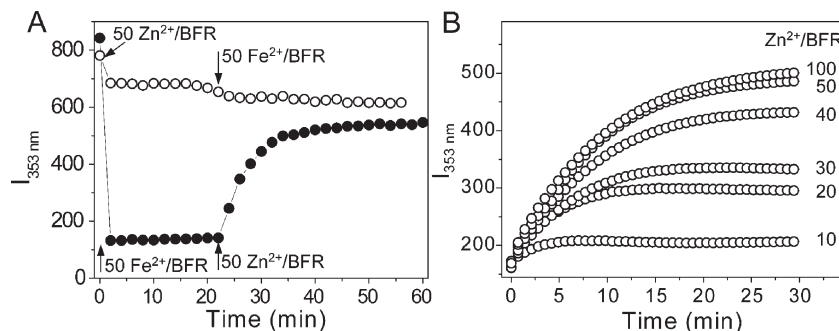


FIGURE 8: Displacement of Fe^{3+} ions from the ferroxidase center of BFR by Zn^{2+} ions. (A) Plots of emission intensity at 353 nm of wild-type BFR as a function of time following addition of 50 Zn^{2+} ions followed by 50 Fe^{2+} ions per BFR (\circ), and, to a separate sample, 50 Fe^{2+} ions followed by 50 Zn^{2+} ions per BFR (\bullet). Both experiments were conducted under aerobic conditions. Arrows indicate the time points at which metal ion additions were made. (B) Emission intensity at 353 nm following the addition of variable amounts of Zn^{2+} ions (as indicated) to BFR already containing 50 Fe^{3+} ions (added as Fe^{2+} ions under aerobic conditions with a 5 min incubation time between metal ion additions). BFR ($0.1 \mu\text{M}$) was in 0.1 M Mes (pH 6.5), at 25°C . Excitation was at 290 nm (with excitation and emission slits of 12 and 6 nm, respectively).

Although the W35F/W133F BFR variant contains no tryptophan residues, each subunit still contains seven tyrosine residues. Therefore, we investigated whether Fe^{2+} binding and oxidation might be followed through the tyrosine fluorescence (which is normally not observed in the wild-type protein). Figure 7C shows changes in the fluorescence emission spectrum as Fe^{2+} was added. Although the extent of the quench was not as great as observed in the wild-type protein ($\sim 50\%$ of the original intensity at 310 nm remained, compared to $\sim 20\%$ for the wild type at 353 nm), the shape of the plot was very similar (inset, Figure 7C). Thus, quenching of fluorescence intensity does not appear to be residue specific. Two tyrosines, Tyr25 and Tyr58, lie within 6.5 Å of the ferroxidase center, and it is highly likely that they are important for the sensitivity of the tyrosine fluorescence intensity to the iron status of the ferroxidase center and may also be important for the sensitivity of Trp133, via a FRET mechanism similar to that proposed to connect the two tryptophan residues (see above).

Fluorescence-Detected Displacement of Iron from the BFR Ferroxidase Center. We have shown here that binding of Fe^{2+} ions to BFR under aerobic conditions leads to a major quench of the tryptophan fluorescence intensity, due to contributions from both Fe^{2+} binding and oxidation. It is well established that Zn^{2+} ions can inhibit core formation in BFR by binding tightly at the ferroxidase center (6, 17), and we recently determined the structure of a Zn^{2+} -bound form of BFR, which revealed Zn^{2+} at the center (and nowhere else) (5). Therefore, it was of interest to assess the effect of Zn^{2+} on BFR fluorescence intensity. The addition of 50 Zn^{2+} ions per BFR resulted in a small quench, to $\sim 85\%$ of the original intensity (see Figure 8A). The addition of 50 Fe^{2+} ions to the same sample resulted in only a minor decrease in fluorescence intensity, consistent with the ability of Zn^{2+} to effectively block Fe^{2+} binding at the ferroxidase center. This also demonstrates that the fluorescence intensity is not very sensitive to Fe^{2+} bound at locations other than the ferroxidase center. Our recent crystallographic studies showed that, when Zn^{2+} ions occupy the ferroxidase center, Fe^{2+} ions can still bind to a novel inner surface site, which itself is ~ 10 Å from the ferroxidase center (5).

The effect of Zn^{2+} on a sample of BFR already containing 50 Fe^{3+} ions (added as Fe^{2+} ions under aerobic conditions) was also investigated. Figure 8A shows that the quench resulting from the binding and oxidation of Fe^{2+} ions was reversed upon addition of 50 Zn^{2+} ions per BFR, recovering to $\sim 70\%$ of the original intensity over a period of ~ 30 min. Thus, the data demonstrate that the fluorescence intensity is sensitive not only to iron binding at the ferroxidase center but also to it leaving the center and is, therefore, a sensitive probe of the iron status of the center. That a full recovery of the intensity relative to that observed for 50 Zn^{2+} ions per BFR was not observed indicated either that Zn^{2+} could not displace all of the Fe^{3+} or that the displaced Fe^{3+} maintained some capacity to quench the fluorescence intensity. To investigate this further, a titration of BFR already containing 50 Fe^{3+} ions (added as Fe^{2+} ions under aerobic conditions) with variable amounts of Zn^{2+} was performed (see Figure 8B). This showed that the extent of the recovery was dependent on the ratio of Zn^{2+} added, and that it was saturated at a level of ~ 50 Zn^{2+} ions per BFR. This indicates that Zn^{2+} is able to displace all of the iron from the ferroxidase center, resulting in a di- Zn^{2+} form of the ferroxidase center, consistent with mechanistic studies that demonstrated that Zn^{2+} is an effective inhibitor of mineralization in BFR even when it contains a significant iron core (10), and

with recent structural studies (5). Therefore, the fact that 100% recovery of the fluorescence intensity was not observed is most likely due to quenching by the displaced Fe^{3+} .

Mechanistic Implications. The specific sensitivity of the BFR fluorescence signal to the iron status of the ferroxidase center provides a useful mechanistic probe. Following phase 2 oxidation of Fe^{2+} at the ferroxidase centers, the fluorescence intensity did not recover (Figure 2D), consistent with the bridged di- Fe^{3+} form of the ferroxidase center in BFR being stable (3, 5, 7, 8, 10). The data are not consistent with a mechanism in which the ferroxidase center acts as a gated pore for transfer of iron into the protein cavity (21, 22). If such a mechanism were in operation, we would expect to observe a substantial recovery of fluorescence intensity following oxidation of Fe^{2+} at the ferroxidase center as the iron passes into the central cavity. Such a recovery was observed for mammalian H-chain ferritin (11), in which a gated pore mechanism does operate (9, 23).

Recovery of fluorescence intensity was observed, albeit slowly, following addition of Zn^{2+} , a potent inhibitor of the ferroxidase center, consistent with displacement of Fe^{3+} at the ferroxidase center by Zn^{2+} , and the extent of the observed recovery was dependent on the amount of Zn^{2+} added, becoming saturated at 2 Zn^{2+} ions per BFR subunit. These data demonstrate that the lability of Fe^{3+} from the ferroxidase center is relatively low, and that the ferroxidase center does not have a very high affinity for Fe^{3+} . From this, we would predict that the redox potential of the $\text{Fe}^{3+}/\text{Fe}^{2+}$ couple at the ferroxidase center is not particularly low, consistent with a previous report that Fe^{3+} at the ferroxidase center iron was readily reduced by ascorbate ($E_m = 53$ mV vs NHE at pH 7) (24). These are properties that might be anticipated for a di-iron catalytic center that can readily cycle between oxidized and reduced states.

Concluding Remarks. Trp133, lying within 10 Å of the ferroxidase center, sensitizes the overall fluorescence of the protein to Fe^{2+} binding and oxidation at the ferroxidase center (i.e., phases 1 and 2 of core mineralization). We propose that this occurs via a resonance energy transfer mechanism between Trp133 and the other tryptophan of the BFR subunit, Trp35, which lies ~ 12 Å from Trp133 and ~ 20 Å from the ferroxidase center. In the absence of Trp133, resonance energy transfer cannot occur by this mechanism and the fluorescence intensity is much less sensitive to iron. The data presented here are consistent with the stability of the di- Fe^{3+} form of the ferroxidase center, as recently demonstrated structurally (5), further supporting a mechanism in which the ferroxidase center does not operate as a gated iron pore. Finally, fluorescence spectroscopy is sensitive not only to Fe^{2+} binding and oxidation at the center but also to the exit of iron from the center, opening up its potential use in studying BFR variants with altered ferroxidase center properties.

ACKNOWLEDGMENT

We thank Nick Cull for excellent technical assistance and the Wellcome Trust for supporting Biophysical Chemistry at the University of East Anglia through an award from the Joint Infrastructure Fund for equipment.

SUPPORTING INFORMATION AVAILABLE

Data refinement and statistics for the structures of W35F and W133F BFRs (Table S1) and sensitivities of the fluorescence intensity of BFR single-tryptophan variants to Fe^{2+} (Figure S1).

This material is available free of charge via the Internet at <http://pubs.acs.org>.

REFERENCES

1. Chasteen, N. D. (1998) Ferritin. Uptake, storage, and release of iron. *Met. Ions Biol. Syst.* **35**, 479–514.
2. Theil, E. C. (1990) The Ferritin Family of Iron Storage Proteins. *Adv. Enzymol. Relat. Areas Mol. Biol.* **63**, 421–449.
3. Lewin, A., Moore, G. R., and Le Brun, N. E. (2005) Formation of protein-coated iron minerals. *Dalton Trans.*, 3597–3610.
4. Cheesman, M. R., Thomson, A. J., Greenwood, C., Moore, G. R., and Kadir, F. (1990) Bis-Methionine Axial Ligation of Heme in Bacterioferritin from *Pseudomonas aeruginosa*. *Nature* **346**, 771–773.
5. Crow, A., Lawson, T. L., Lewin, A., Moore, G. R., and Le Brun, N. E. (2009) Structural basis for iron mineralization by bacterioferritin. *J. Am. Chem. Soc.* **131**, 6808–6813.
6. Le Brun, N. E., Andrews, S. C., Guest, J. R., Harrison, P. M., Moore, G. R., and Thomson, A. J. (1995) Identification of the ferroxidase centre of *Escherichia coli* bacterioferritin. *Biochem. J.* **312**, 385–392.
7. Le Brun, N. E., Wilson, M. T., Andrews, S. C., Guest, J. R., Harrison, P. M., Thomson, A. J., and Moore, G. R. (1993) Kinetic and Structural Characterization of an Intermediate in the Biomineralization of Bacterioferritin. *FEBS Lett.* **333**, 197–202.
8. Yang, X., Le Brun, N. E., Thomson, A. J., Moore, C. R., and Chasteen, N. D. (2000) The iron oxidation and hydrolysis chemistry of *Escherichia coli* bacterioferritin. *Biochemistry* **39**, 4915–4923.
9. Zhao, G. H., Bou-Abdallah, F., Arosio, P., Levi, S., Janus-Chandler, C., and Chasteen, N. D. (2003) Multiple pathways for mineral core formation in mammalian apoferritin. The role of hydrogen peroxide. *Biochemistry* **42**, 3142–3150.
10. Baaghil, S., Lewin, A., Moore, G. R., and Le Brun, N. E. (2003) Core formation in *Escherichia coli* bacterioferritin requires a functional ferroxidase center. *Biochemistry* **42**, 14047–14056.
11. Cavallo, S., Mei, G., Stefanini, S., Rosato, N., Finazzi-Agro, A., and Chiancone, E. (1998) Formation and movement of Fe(III) in horse spleen, H- and L-recombinant ferritins: A fluorescence study. *Protein Sci.* **7**, 427–432.
12. Sambrook, J., Fritsch, F. E., and Maniatis, T. (1989) Molecular Cloning: A Laboratory Manual, 2nd ed., Cold Spring Harbor Laboratory Press, Plainview, NY.
13. Hutchings, M. I., Shearer, N., Wastell, S., Van Spanning, R. J. M., and Spiro, S. (2000) Heterologous NMR-mediated nitric oxide signaling in *Escherichia coli*. *J. Bacteriol.* **182**, 6434–6439.
14. Bauminger, E. R., Harrison, P. M., Hechel, D., Nowik, I., and Treffry, A. (1991) Mössbauer spectroscopic investigation of structure-function relations in ferritins. *Biochim. Biophys. Acta* **1118**, 48–58.
15. Malone, S. A., Lewin, A., Kilic, M. A., Svistunenko, D. A., Cooper, C. E., Wilson, M. T., Le Brun, N. E., Spiro, S., and Moore, G. R. (2004) Protein-template-driven formation of polynuclear iron species. *J. Am. Chem. Soc.* **126**, 496–504.
16. DeLano, W. L. (2002) PyMOL, DeLano Scientific, San Carlos, CA.
17. Le Brun, N. E., Keech, A. M., Mauk, M. R., Mauk, A. G., Andrews, S. C., Thomson, A. J., and Moore, G. R. (1996) Charge compensated binding of divalent metals to bacterioferritin: H⁺ release associated with cobalt(II) and zinc(II) binding at dinuclear metal sites. *FEBS Lett.* **397**, 159–163.
18. Wong, S. G., Tom-Yew, S. A., Lewin, A., Le Brun, N. E., Moore, G. R., Murphy, M. E., and Mauk, A. G. (2009) Structural and mechanistic studies of a stabilized subunit dimer variant of *Escherichia coli* bacterioferritin identify residues required for core formation. *J. Biol. Chem.* **284**, 18873–18881.
19. Aitken-Rogers, H., Singleton, C., Lewin, A., Taylor-Gee, A., Moore, G. R., and Le Brun, N. E. (2004) Effect of phosphate on bacterioferritin-catalysed iron(II) oxidation. *J. Biol. Inorg. Chem.* **9**, 161–170.
20. Lakowicz, J. R. (1999) Principles of Fluorescence Spectroscopy, Kluwer Academic/Plenum Publishers, New York.
21. Macedo, S., Romao, C. V., Mitchell, E., Matias, P. M., Liu, M. Y., Xavier, A. V., LeGall, J., Teixeira, M., Lindley, P., and Carrondo, M. A. (2003) The nature of the di-iron site in the bacterioferritin from *Desulfovibrio desulfuricans*. *Nat. Struct. Biol.* **10**, 285–290.
22. Swartz, L., Kuchinskas, M., Li, H. Y., Poulos, T. L., and Lanzilotta, W. N. (2006) Redox-dependent structural changes in the *Azotobacter vinelandii* bacterioferritin: New insights into the ferroxidase and iron transport mechanism. *Biochemistry* **45**, 4421–4428.
23. Bou-Abdallah, F., Zhao, G. H., Mayne, H. R., Arosio, P., and Chasteen, N. D. (2005) Origin of the unusual kinetics of iron deposition in human H-chain ferritin. *J. Am. Chem. Soc.* **127**, 3885–3893.
24. Le Brun, N. F., Cheesman, M. R., Thomson, A. J., Moore, G. R., Andrews, S. C., Guest, J. R., and Harrison, P. M. (1993) An EPR investigation of non-heme iron sites in *Escherichia coli* bacterioferritin and their interaction with phosphate: A study using nitric oxide as a spin probe. *FEBS Lett.* **323**, 261–266.